Robust fractional-order control of PMSG-based WECS

Sajjad Shoja-Majidabad*

Electrical Engineering Department,
Bonab University,
East Azerbaijan, Bonab, Iran
Email: shoja.sajjad@gmail.com
*Corresponding author

Heydar Toosian-Shandiz and Amin Hajizadeh

Faculty of Electrical Engineering,
Shahrood University of Technology,
Semnan, Shahrood, Iran
Email: htshandiz@shahroodut.ac.ir
Email: aminhajizadeh@shahroodut.ac.ir

Abstract: This paper presents some novel fractional-order nonlinear sliding mode controllers for maximum power extraction of a grid-connected wind energy conversion system. Two similar fractional-order controllers with nonlinear sliding manifolds are proposed for generator-side and grid-side converters. The main role of the generator-side controller is regulating the mechanical speed of wind turbine to follow an optimum speed. On the other hand, the grid-side controller main goal is governing the active and reactive power by tuning DC-link voltage. Practical stability of both controllers is achieved by fractional-order nonlinear stability theorems. Comparative simulations are presented to show the effectiveness of the proposed controllers.

Keywords: wind energy conversion system; WECS; fractional-order nonlinear sliding mode control; permanent magnet synchronous generator.

Reference to this paper should be made as follows: Shoja-Majidabad, S., Toosian-Shandiz, H. and Hajizadeh, A. (xxxx) 'Robust fractional-order control of PMSG-based WECS', *Int. J. Automation and Control*, Vol. X, No. Y, pp.xxx–xxx.

Biographical notes: Sajjad Shoja-Majidabad received his BSc from Sahand University of Technology, Tabriz, Iran in 2008, MSc and PhD in Electrical Engineering from the Shahrood University of Technology, Shahrood, Iran in 2010 and 2014. Currently, he is an Assistant Professor in the Faculty of Electrical Engineering at the Bonab University. His research interests include: nonlinear robust control, fractional-order control, power system analysis and control, and intelligent control.

Heydar Toosian-Shandiz received his PhD degree from UMIST University. He is an Associate Professor in the Shahrood University of Technology. His research interests include: fractional calculus, industrial automation and control, intelligent computing, digital signal processing (DSP), systems identification, adaptive systems and information technology.

Copyright © 20XX Inderscience Enterprises Ltd.

Amin Hajizadeh received his BSc degree from Ferdowsi University of Mashahd, Mashad, Iran in 2002, and MSc and PhD degree in Electrical Engineering from the K.N. Toosi University of Technology, Tehran, Iran in 2005 and 2010. During February 2009 until August 2009, he worked as a Visiting PhD student with the Department of Electrical Power Engineering at the Norwegian University of Science and Technology (NTNU), Trondheim, Norway. Currently, he is an Assistant Professor at the Shahrood University of Technology in Shahrood, Iran. His current research interests include: control of distributed energy resources and grid-connected operation of hybrid power systems and distributed generation.

1 Introduction

Nowadays, wind power is most rapidly growing renewable and clean energy source. A wind energy conversion system (WECS) operates either at a constant or variable speed. A variable speed wind turbine is more interesting than a constant speed turbine mainly because of the maximum power point tracking (MPPT) capability. The variable speed turbines are usually based on doubly fed induction generators (DFIGs) or permanent magnet synchronous generators (PMSGs). The application of the PMSG-based wind turbine has increased due to the efficient energy production and simple structure (Li et al., 2012; Morimoto et al., 2005; Chinchilla et al., 2006; Uehara et al., 2011).

So far, many valuable control techniques have been reported for the maximum power extraction of the PMSG-based WECS. For instance, proportional integral (PI) control (Li et al., 2012; Morimoto et al., 2005; Chinchilla et al., 2006; Uehara et al., 2011; Kasem-Alaboudy et al., 2012), feedback linearisation technique (Qiao et al., 2009), gain scheduling (Bianchi et al., 2007), fuzzy control (Eltamaly and Farh, 2013; Aissaoui et al., 2013), neural networks approach (Cadenas and Rivera, 2009), and some sensorless control techniques (Thongam et al., 2012; Qiao et al., 2012) have been developed to deal with the control of the PMSG-based WECS. In addition, in order to have a robust response against model uncertainties, the conventional sliding mode control (SMC) and its higher-order forms have been presented in Lin et al. (2011), Corradini et al. (2012), Valenciaga and Puleston (2008), Beltran et al. (2009) and Benelghali et al. (2011). It is rewarding to note that all the mentioned studies have been designed based on the integer calculus.

Fractional calculus idea was established in the 17th century. This field of mathematic discusses about arbitrary-order derivatives and integrals. For three centuries, this topic was developed as a pure theoretical subject with no applications (Podlubny, 1999). However, in recent years, the fractional calculus has been applied in different branches of engineering and science, such as finance systems (Laskin, 2000), biological systems (Petras and Magin, 2011), thermoelectric systems (Ezzat, 2011), reaction-diffusion systems (Gafiychuk et al., 2008), electrical circuits (Luo et al., 2011), rotor-bearing systems (Cao et al., 2011) and so on. In addition, fractional-order control of integer-order systems is another important application of the fractional calculus. Compared with integer-order controllers, fractional-order controllers provide some extra tuning parameters, which may provide a better closed-loop performance (Chen, 2006).

To enhance the conventional SMC's performance, combining it with the fractional calculus found so interesting. This combination is called fractional-order sliding mode

control (FoSMC). Recently, the FoSMC applications have been reported in various literatures such as: robot manipulators (Efe, 2008), permanent magnet synchronous motors (Zhang et al., 2012), antilock braking systems (Tang et al., 2012), induction motors (Chang et al., 2011), vibration suppression (Aghababa, 2013), cognitive lighting control (Yin et al., 2013), and PMSG-based WECS (Melicio et al., 2010). All of these studies (except Yin et al., 2013) are common in employing a linear sliding surface. But the linear sliding surface shows a slow response with a considerable tracking error. To attenuate the mentioned drawbacks, the FoSMC with a nonlinear sliding surface has been presented in a few references (Dadras and Momeni, 2012; Aghababa, 2013) for nonlinear systems. This technique is known as the fractional-order nonlinear sliding mode control (FoNSMC). Fast response and low tracking error are dominant specifications of the FoNSMC.

In this paper, two novel forms of the FoNSMCs are designed for mechanical speed and DC-link voltage in order to extract maximum power. Our proposed controllers provide three extra adjusting parameters to reach a fast and high precision response. The controllers are verified by fractional-order nonlinear stability theorems.

This paper is organised as follows: Section 2 expresses the dynamic model and configuration of WECS. Section 3 presents some preliminaries from fractional calculus. Section 4 develops the FoNSMC and presents the stability analysis. Section 5 provides the simulation results and some comparisons with the conventional SMC base controllers. Finally, Section 6 concludes the paper.

2 WECS modelling

The WECS consists mainly of three parts: a wind turbine, a PMSG, and two back-to-back converters which are connected through a DC-link. The configuration of the whole system is described in Figure 1.

Figure 1 Configuration of the PMSG-based WECS (see online version for colours)

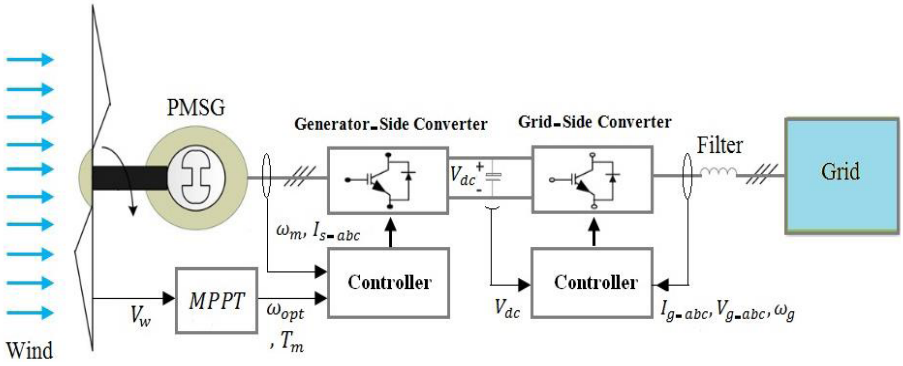

2.1 Wind turbine model

The mechanical power captured by a wind turbine can be expressed as (Li et al., 2012; Kasem-Alaboudy et al., 2012):

$$P_m = \frac{1}{2} C_p(\beta, \lambda) \rho \pi r^2 V_w^2 \tag{1}$$

where ρ is the air density (kg/m^3), r is the radius of the turbine blades (m), V_w is the wind speed (m/s) and $C_p(\beta, \lambda)$ is the power coefficient which is a function of the tip speed ratio λ and pitch angle β, of the blades. In this paper, we assumed that the pitch angle β, be zero, which is a reasonable assumption for low and medium wind speeds. In addition, the tip speed ratio is given by

$$\lambda = \frac{r\omega_t}{V_w} \tag{2}$$

where ω_t is the turbine shaft rotational speed (rad/s).

The turbine mechanical torque can be obtained as:

$$T_m = \frac{P_m}{\omega_t} \tag{3}$$

2.2 PMSG transient model

Generally, the dynamic model of a PMSG is the same as a permanent magnet synchronous motor (PMSM) (Uehara et al., 2011). The voltages of the PMSM in the dq-reference frame are given by (Li et al., 2012; Kasem-Alaboudy et al., 2012):

$$v_{sd} = R_s I_{sd} + L_{sd} \frac{dI_{sd}}{dt} - L_{sq} \omega_e I_{sq} \tag{4}$$

$$v_{sq} = R_s I_{sq} + L_{sq} \frac{dI_{sq}}{dt} + L_{sd} \omega_e I_{sd} + \omega_e \varphi_f \tag{5}$$

where R_s is the resistance of the stator winding, L_{sd} and L_{sq} are the generator winding dq-axis inductances, ω_e is the generator electrical rotational speed, φ_f is the flux linkage produced by the permanent magnet, v_{sd} and v_{sq} are the dq-axis voltages, I_{sd} and I_{sq} are the dq-axis currents.

The electrical torque is given by from the following expression:

$$T_e = \frac{3}{2} p \left[\varphi_f I_{sq} + \left(L_{sd} - L_{sq} \right) I_{sd} I_{sq} \right] \tag{6}$$

where p is the number of pole pairs. Generating operation starts when the torque T_e is negative.

For a surface mounted PMSG, L_{sd} and L_{sq} are quiet similar ($L_{sd} = L_{sq} = L$). Then, the equation (6) can be simplified as:

$$T_e = K I_{sq} \tag{7}$$

where

$$K = \frac{3}{2} p\varphi_f .$$

The mechanical speed dynamic of a gearless machine ($\omega_m = \omega_t$) is described by:

$$T_e = J\frac{d\omega_m}{dt} + F\omega_m + T_m \tag{8}$$

where J is the inertia of the whole system including the generator and turbine (Kg.m^2). F is the rotational damping (N.m.sec), and ω_m is the mechanical angular velocity of the generator rotor ($\omega_e = p\omega_m$).

2.3 Power electronic converters and vector control

In wind turbines, the back-to-back converters are widely utilised. The first converter is known as the generator-side converter, which is connected to the DC-link, and its dominant duty is converting the AC to DC signal. In the other word, the converter acts as a rectifier. The second converter is named the grid-side converter, which transforms the DC to AC signal. In this case, the converter acts as an inverter. Generally, the generator-side converter controls the mechanical speed, while the grid-side converter keeps the DC-link voltage constant and manages the delivered active and reactive power.

2.3.1 Generator-side converter

Based on (1), the maximum extracted power depends on the power coefficient $C_p(0, \lambda)$, while this coefficient is not constant for different wind speeds. The turbine must operate in $C_{p\text{-}max}$ in order to capture the maximum power (Kasem-Alaboudy et al., 2012). On the other hand, there is an optimum tip speed ratio λ_{opt} that leads to maximum power coefficient $C_{p\text{-}max}$. The ratio λ_{opt} is corresponds to an optimal speed ω_{opt}. Therefore, it is important to keep the mechanical speed ω_m at the optimal speed ω_{opt} which is produced by MPPT block. If the optimum speed fluctuates, ω_m should be tuned to track the fluctuations. The mentioned idea is realisable by controlling the generator-side converter.

Substituting (7) in (8), results in

$$\frac{d\omega_m}{dt} = \frac{1}{J}\left(KI_{sq} - F\omega_m - T_m\right) \tag{9}$$

From (9), it is obvious that the mechanical speed ω_m is related to the quadrature current component I_{sq}. Then, the speed ω_m can be controlled by changing I_{sq}. In addition, the direct current component I_{sd} should be set zero to minimise the resistive losses. We selected two PI controllers to converge the currents I_{sd} and I_{sq} to the reference values ($I_{sd\text{-}ref}$ = 0and $I_{sq\text{-}ref}$). More details about the generator-side converter control are presented in Figure 2 and the next sections.

Figure 2 Generator-side converter control (see online version for colours)

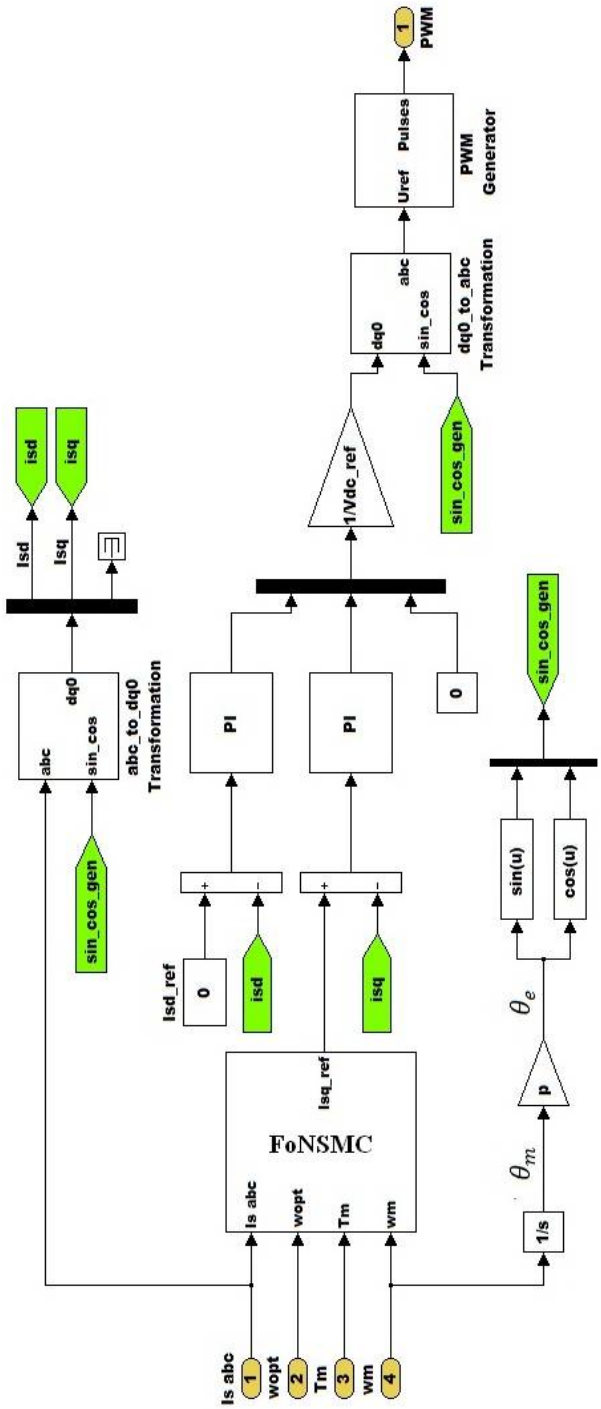

2.3.2 Grid-side converter

The dynamic model of the grid-side converter in *dq*-reference frame is expressed as (Chinchilla et al., 2006):

$$V_{gd} = u_d - R_g I_{gd} - L_g \frac{dI_{gd}}{dt} + L_g \omega_g I_{gq} \tag{10}$$

$$V_{gq} = u_q - R_g I_{gq} - L_g \frac{dI_{gq}}{dt} - L_g \omega_g I_{gd} \tag{11}$$

where R_s and L_g are the supply side resistance and inductance, respectively, I_{gd} and I_{gq} are the direct and quadrature components of the grid-side converter currents, and u_d and u_q are the grid voltage components.

With the reference frame oriented along the grid voltage ($V_g = V_{gd} + j0$), the active and reactive power can be given and simplified as follows:

$$P_g = \frac{3}{2}\left(V_{gd} I_{gd} + V_{gq} I_{gq}\right) = \frac{3}{2} V_{gd} I_{gd} \tag{12}$$

$$Q_g = \frac{3}{2}\left(V_{gd} I_{gq} - V_{gq} I_{gd}\right) = \frac{3}{2} V_{gd} I_{gq} \tag{13}$$

From (12) and (13), it is evident that the active and reactive power (P_g and Q_g) can be controlled by changing the *dq*-current components. Generally, applying two internal current-control-loops is a proper method in order to control the active and reactive power.

On the other hand, the DC-link voltage should remain constant in order to transfer all the active power produced by the turbine. Using the power balance principle and neglecting the converter losses, the dynamic behaviour of the DC-link voltage V_{dc} can be written as:

$$\frac{dV_{dc}}{dt} \cong \frac{P_t}{CV_{dc}} - \frac{P_g}{CV_{dc}} \tag{14}$$

Using (12), equation (14), will be as

$$\frac{dV_{dc}}{dt} \cong \frac{P_t}{CV_{dc}} - \frac{3V_{gd}}{2CV_{dc}} I_{gd} \tag{15}$$

From (15), it is apparent that the voltage V_{dc} is governable by controlling the direct current I_{gd}. This goal is achievable by considering I_{gd} as a reference signal to the internal current-control-loop. The global grid-side converter control configuration which is used in this study is illustrated in Figure 3. Also, more explanations are presented in Section 4.

Figure 3 Grid-side converter control (see online version for colours)

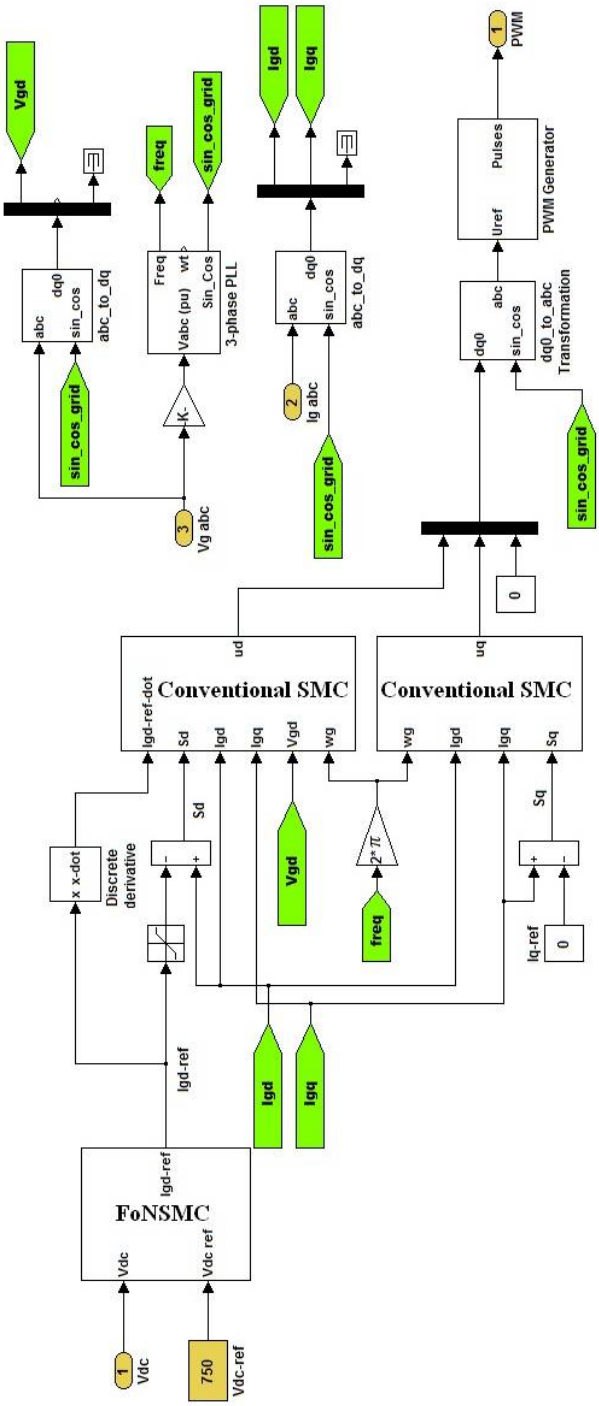

3 Fractional calculus preliminaries

In this section, some useful definitions, properties and theorem of the fractional calculus are expressed.

Definition 1 (Hewitt and Stromberg, 1965): The $f(t)$: $\mathbb{R} \to \mathbb{R}$ function is continuously differentiable if $f(t)$ be differentiable and $\dot{f}(t)$ be continuous.

From this definition, $f(t) \in C^0$, C^1 are the classes of all continuous and continuously differentiable functions, respectively.

Definition 2 (Li and Deng, 2007): The α^{th} order Riemann-Liouville fractional integration of function $f(t)$ with respect to t is given by

$$I_{0,t}^{\alpha} f(t) = D_{0,t}^{-\alpha} f(t) = \frac{1}{\Gamma(\alpha)} \int_0^t \frac{f(\tau)}{(t-\tau)^{1-\alpha}} d\tau \tag{16}$$

where $\Gamma(\alpha)$ is the Gamma function.

Definition 3 (Li and Deng, 2007): The α^{th} order Caputo fractional derivative of continuous ($f(t) \in C^m$ [0, t]) function $f(t)$ is defined as follows:

$${}_C D_{0,t}^{\alpha} f(t) = D_{0,t}^{-(m-\alpha)} D^m f(t) = \frac{1}{\Gamma(m-\alpha)} \int_0^t \frac{f^{(m)}(\tau)}{(t-\tau)^{1-m+\alpha}} d\tau \tag{17}$$

where $m - 1 < \alpha < m$, $m \in \mathbb{N}$.

Property 1 (Li and Deng, 2007): If $f(t) \in C^0$ [0, T] for $T > 0$ and $\alpha > 0$, then $D_{0,t}^{-\alpha} f(t)|_{t=0} = 0$.

Property 2 (Li and Deng, 2007): If $(t) \in C^1$ [0,∞), $0 < \alpha < 1$, then ${}_C D_{0,t}^{\alpha} D_{0,t}^{-\alpha} f(t) = f(t)$.

Property 3 (sequential property) (Shoja-Majidabad et al., 2014): If $s(t) \in C^1$ [0, T] for some $T > 0$, $\alpha_i \in (0, 1)$ ($i = 1, 2$) and $\alpha_1 + \alpha_2 \in (0, 1]$, then

$${}_C D_{0,t}^{\alpha_1} {}_C D_{0,t}^{\alpha_2} (t) = {}_C D_{0,t}^{\alpha_2} {}_C D_{0,t}^{\alpha_1} s(t) = {}_C D_{0,t}^{\alpha_1+\alpha_2} s(t) \tag{18}$$

Theorem 1 (Li et al., 2010): Let $x = 0$ be an equilibrium point for the non-autonomous fractional-order system

$${}_C D_{0,t}^{\alpha} x(t) = f\left(t, x(t)\right) \tag{19}$$

where $f(t, x(t))$ satisfies the Lipschitz condition with the Lipschitz constant $l > 0$ and $\alpha \in (0, 1)$. Assume that there exists a Lyapunov function $V(t, x(t))$ satisfying

$$\alpha_1 \| x \|^a \le V\left(t, x(t)\right) \le \alpha_2 \| x \| \tag{20}$$

$$\frac{d}{dt} V\left(t, x(t)\right) \le -\alpha_3 \| x \| \tag{21}$$

where α_1, α_2, α_3 and a are positive constants. Then the equilibrium point of the system (19) is asymptotically stable.

Remark 1: Sequential property is an attractive tool for the FoSMC technique. But the continuously differentiability condition restricts this property. To clarify this concept, consider $\alpha_1 = \alpha$ and $\alpha_2 = 1 - \alpha$, then the equation (18) can be written as:

$$\dot{s}(t) = {}_C D^{\alpha}_{0,t} {}_C D^{1-\alpha}_{0,t} s(t) = {}_C D^{1-\alpha}_{0,t} {}_C D^{\alpha}_{0,t} s(t) \tag{22}$$

from mathematical point of view and according to Property 3, equation (22) holds for continuous $s(t)$ and $\dot{s}(t)$. However, discontinuous sgn($s(t)$) function, non-smooth desired signals and sudden changes in the disturbance can cause $\dot{s}(t)$ discontinuity, which degrades C^1 condition. Using fuzzy approximations, smooth functions $(\tanh(s(t)), sat(s(t)), D^{-\alpha}_{0,t}(s(t)))$ instead of sgn($s(t)$) and smooth desired signals are approximate practical remedies for the mentioned problem.

4 Fractional-order nonlinear sliding mode control of the power converters

In this section, two FoNSMCs are designed for the generator-side and the grid-side converters in order to control mechanical speed and regulate the DC-link voltage, respectively. Both of the controllers are on the outer-loop and they generate reference signals for the internal current-control-loops.

4.1 Generator-side converter control

The mechanical speed dynamic (9), can be rewritten as:

$$\dot{\omega}_m(t) = -a\omega_m(t) - bT_m(t) + cI_{sq}(t) \tag{23}$$

where the parameters are given by:

$$a = \frac{B}{J}, \quad b = \frac{1}{J}, \quad c = \frac{K}{J} \tag{24}$$

Now, by considering the uncertainties and parameter variations, the equation (24) will be as follows:

$$\dot{\omega}_m(t) = -\left(\hat{a} + \Delta a\right)\omega_m(t) - \left(\hat{b} + \Delta b\right)T_m(t) + \left(\hat{c} + \Delta c\right)I_{sq}(t) \tag{25}$$

where $\hat{a}$, $\hat{b}$ and $\hat{c}$ represent the estimated values, and Δa, Δb and Δc are unknown uncertainty terms of parameters a, b and c. By defining the global uncertainty term $M(t) = -\Delta a\omega_m(t) - \Delta bT_m(t) + \Delta cI_{sq}(t)$, the mechanical speed dynamic (25) can be rearranged in the following form:

$$\dot{\omega}_m(t) = -\hat{a}\omega_m(t) - \hat{b}T_m(t) + \hat{c}I_{sq}(t) + M(t) \tag{26}$$

Assumption 1: Assume that the uncertainty term $M(t)$ satisfies the following condition:

$$\left|{}_C D^{1-\alpha_1} M(t)\right| \le \delta_1 \tag{27}$$

where δ_1 is a positive and known constant.

Now, by defining the speed tracking error $e_m(t) = \omega_{opt}(t) - \omega_m(t)$, we propose the nonlinear sliding surface in the following form:

$$s_\omega(t) = {}_C D^{1-\alpha_1} e_m(t) + \gamma_1 D^{-\alpha_1} e_m^{\mu_1}(t) \tag{28}$$

where $\omega_{opt}(t)$ is the reference speed, $0 < \alpha_1 < 1$, $\gamma_1 > 0$, and $0 < \mu_1 < 1$ is a rational number with odd numerator and denumerator.

Taking ${}_C D^{\alpha_1}$ derivative from (28), yields

$${}_C D^{\alpha_1} s_\omega(t) = {}_C D^{\alpha_1}{}_C D^{1-\alpha_1} e_m(t) + \gamma_1 {}_C D^{\alpha_1} D^{-\alpha_1} e_m^{\mu_1}(t) \tag{29}$$

and using Properties 2 and 3, we can get

$${}_C D^{\alpha_1} s_\omega(t) = \dot{e}_m(t) + \gamma_1 e_m^{\mu_1}(t) \tag{30}$$

Substituting (26) in (30), results in

$${}_C D^{\alpha_1} s_\omega(t) = \dot{\omega}_{opt}(t) + \hat{a}\omega_m(t) + \hat{b}T_m(t) + \gamma_1 e_m^{\mu_1}(t) - \hat{c}I_{sq}(t) + M(t) \tag{31}$$

Theorem 2: Consider the mechanical speed dynamic (26) with the nonlinear sliding manifold (28) and Assumption 1, then the following control law

$$\begin{aligned} I_{sq}(t) = \frac{1}{\hat{c}}\Big(& \hat{a}w_m(t) + \hat{b}T_m(t) + \gamma_1 e_m^{\mu_1}(t) + \dot{w}_{opt}(t) + D^{-(1-a_1)} \\ & \left(\eta_1 s_w(t) + K_{sw1}\tanh\left(s_w(t)/\varepsilon_1\right)\right)\Big) \end{aligned} \tag{32}$$

guarantees the speed tracking error convergence. Where η_1 is a positive constant, ε_1 is an enough small positive constant, K_{sw} is the switching gain which satisfies $K_{sw1} = \delta_1 \ge |{}_C D^{1-\alpha_1} M(t)|$, and tanh(·) is the hyperbolic tangent function.

Stability proof: Let us define the following Lyapunov function:

$$V(t) = \left|s_\omega(t)\right| \tag{33}$$

The time derivative of $V(t)$ can be calculated as:

$$\dot{V}(t) = \operatorname{sgn}\left(s_\omega(t)\right)\dot{s}_\omega(t) \tag{34}$$

Based on Property 3, we have

$$\dot{V}(t) = \operatorname{sgn}\left(s_\omega(t)\right)\dot{s}_\omega(t) = \operatorname{sgn}\left(s_\omega(t)\right)\ {}_C D^{1-\alpha_1}\,{}_C D^{\alpha_1} s_\omega(t) \tag{35}$$

Substituting (31) and (32) into (35), yields

$$\begin{aligned}\dot{V}(t) &= \operatorname{sgn}\left(s_\omega(t)\right)\ {}_C D^{1-\alpha_1}\left(M(t) - {}_C D^{-(1-\alpha_1)}\left(\eta_1 s_\omega(t) + K_{sw1}\tanh\left(s_\omega(t)/\varepsilon_1\right)\right)\right)\\ &= \operatorname{sgn}\left(s_\omega(t)\right)\left({}_C D^{1-\alpha_1} M(t) - \eta_1 s_\omega(t) - K_{sw1}\tanh\left(s_\omega(t)/\varepsilon_1\right)\right)\end{aligned} \tag{36}$$

Assuming $\varepsilon_1 \to 0$, results the approximation $\tanh(s_\omega(t)/\varepsilon_1) \cong \operatorname{sgn}(s_\omega(t))$, then we can get

$$\dot{V}(t) \cong \operatorname{sgn}\left(s_\omega(t)\right)\ {}_C D^{1-\alpha_1} M(t) - \eta_1\left|s_\omega(t)\right| - K_{sw1} \tag{37}$$

Selecting the sliding gain $K_{sw1} = \delta_1 \geq \left|{}_C D^{1-\alpha_1} M(t)\right|$, results in

$$\dot{V}(t) \leq -\eta_1\left|s_\omega(t)\right| \tag{38}$$

which guarantees the closed-loop system stability based on Theorem 1. □

Although the control law (32) provides the reference current $I_{sq\text{-}ref}$ for the inner-loop, but this law is not able to guarantee the *dq*-currents convergence. Therefore, two PI controllers are employed for the internal current-control-loops in order to promise the currents convergence. The complete configuration of the generator-side controller is presented in Figure 2. In this figure, $I_{sd\text{-}ref}$ is considered zero to minimise the resistive losses.

Remark 2: Inserting the control law (32) in (31) results the following closed-loop system dynamics

$${}_C D^{\alpha_1} s_\omega(t) = M(t) - D^{-(1-\alpha_1)}\left(\eta_1 s_\omega(t) + K_{sw1}\tanh\left(s_\omega(t)/\varepsilon_1\right)\right) \tag{39}$$

which has fractional-order dynamics and requires fractional-order stability theorems.

4.2 Grid-side converter control

Generally, the goal of the grid-side converter controller is to transfer the maximum active power of the wind turbine to the grid with no reactive power. In this part, the FoNSMC is designed to adjust the DC-link voltage. In addition, the conventional SMC is applied to the internal current-control-loops.

4.2.1 DC-link voltage control

Let us arrange the DC-link voltage dynamic (15) in the following form:

$$\frac{dV_{dc}(t)}{dt} = -H(t)I_{gd}(t) + \frac{P_t(t)}{CV_{dc}(t)} \tag{40}$$

where $\frac{P_t(t)}{V_{dc}(t)}$ is the generator-side converter discontinuous output current, and $H(t) = \frac{3V_{gd}}{2CV_{dc}(t)}$. Now, we can rewrite (40) as follows:

$$\frac{dV_{dc}(t)}{dt} = -H(t)I_{gd}(t) + L(t) \tag{41}$$

where

$$L(t) = \frac{P_t(t)}{CV_{dc}(t)} + P_{losses}(t) \tag{42}$$

is called the lumped uncertainty term.

Assumption 2: Assume that the lumped uncertainty $L(t)$ fulfils the following condition:

$$|\ {}_C D^{1-\alpha_2} L(t)\ | \ \le \delta_2 \tag{43}$$

where δ_2 is a positive and known constant.

Based on (41), consider the following nonlinear sliding surface:

$$s_v(t) = \ {}_C D^{1-\alpha_2} e_v(t) + \gamma_2 D^{-\alpha_2} e_v^{\mu_2}(t) \tag{44}$$

where $e_v(t) = V_{dc\text{-}ref} - V_{dc}(t)$ is the DC-link voltage tracking error, $V_{dc\text{-}ref}$ is the reference voltage, $0 < \alpha_2 < 1$, $\gamma_2 > 0$, and $0 < \mu_2 < 1$ is a rational number with odd numerator and denumerator

By taking ${}_C D^{\alpha_2}$ derivative from both sides of (44) and substituting (41) in it, we can get

$${}_C D^{\alpha_2} s_v(t) = \ H(t)I_{gd}(t) + \gamma_2 e_v^{\mu_2}(t) - L(t) \tag{45}$$

Theorem 3: Consider the DC-link voltage dynamic (41) with the nonlinear sliding manifold (44) and Assumption 2, then the following control law

$$I_{gd}(t) = \frac{-1}{H(t)}\left(\gamma_2 e_v^{\mu_2}(t) + D^{-(1-\alpha_2)}\left(\eta_2 s_v(t) + K_{sw2}\tanh\left(s_v(t)/\varepsilon_2\right)\right)\right) \tag{46}$$

guarantees the DC-link voltage tracking error convergence for $K_{sw2} = \delta_2 \geq \left| {}_C D^{1-\alpha_2} L(t) \right|$. Where η_2 is a positive constant, and ε_2 is an enough small positive constant.

Stability proof: Similar to the previous section. □

Remark 3: The nonlinear terms $\gamma_1 D^{-\alpha_1} e_m^{\mu_1}(t)$ and $\gamma_2 D^{-\alpha_2} e_v^{\mu_2}(t)$ with parameters $\gamma_1 = \gamma_2 = 1$ are only effective for systems with small variation states. But since the variation range of the errors (γ_1 and γ_2) is wide, then selecting enough big values for the parameters γ_1 and γ_2 is necessary. On the other hand, high values of γ_1 and γ_2 may amplify the system chattering. Therefore, these parameters should be selected by considering a trade-off between a better response and low chattering.

Remark 4: It is worthy to note that the suggested FoNSMC controllers will be integer-order if α_1, $\alpha_2 = 1$. This type of controllers is known as the nonlinear sliding mode control (NSMC).

4.2.2 DQ-current control

The dynamic equations (10) and (11) of the grid-side converter can be rearranged as:

$$\frac{dI_{gd}}{dt} = \frac{1}{L_g}\left(u_d - R_g I_{gd} + L_g \omega_g I_{gq} - V_{gd}\right) \tag{47}$$

$$\frac{dI_{gq}}{dt} = \frac{1}{L_g}\left(u_q - R_g I_{gq} - L_g \omega_g I_{gd} - 0\right) \tag{48}$$

Now, consider the following sliding surfaces:

$$S_d = I_{gd} - I_{gd\_ref} \tag{49}$$

$$S_q = I_{gq} - I_{gq\_ref} \tag{50}$$

where I_{gd_ref} and I_{gq_ref} are direct and quadrature desired currents. The quadrature current is selected $I_{gq\_ref} = 0$ in order to achieve the zero reactive power delivery.

The time derivative of the sliding surfaces S_q and S_q can be calculated as:

$$\dot{S}_d = \dot{I}_{gd} - \dot{I}_{gd\_ref} \tag{51}$$

$$\dot{S}_q = \dot{I}_{gq} - 0 \tag{52}$$

Substituting (47) and (48) into (51) and (52), yields

$$\dot{S}_d = -\frac{1}{L_g} V_{gd} - \frac{R_g}{L_g} I_{gd} + \omega_g I_{gq} - \dot{I}_{gd_{ref}} + \frac{1}{L_g} u_d \tag{53}$$

$$\dot{S}_q = -\frac{R_g}{L_g} I_{gq} - \omega_g I_{gd} + \frac{1}{L_g} u_q \tag{54}$$

In order to guarantee the sliding surfaces S_q and S_q convergence, the following current control laws are proposed:

$$u_d = V_{gd} + R_g I_{gd} - L_g \omega_g I_{gq} + L_g \dot{I}_{gd_{ref}} - K_d \operatorname{sgn}(S_d) \tag{55}$$

$$u_q = +R_g I_{gq} + L_g \omega_g I_{gd} - K_d \operatorname{sgn}(S_q) \tag{56}$$

where K_d, $K_q > 0$ are the switching gain parameters.

5 Simulation results

Comparative simulations have been carried out in MATLAB/Simpower environment to verify the effectiveness of the proposed controllers for a 10-kW wind turbine. The sampling time of the simulations is selected T_s = 5 μsec. The simulations are performed for both DC and AC-grid connections.

5.1 WECS connected to the DC-grid

In this state, the grid-side converter is replaced with a 750 volt DC-grid to test the generator-side converter controller performance. In the other word, the generator-side converter is connected to the DC-grid. Three methods (SMC, NSMC, FoNSMC) performances are tested in this case, and the results are presented in Figure 4.

We selected the wind speed variations and the parameters of the tested methods as follows:

Wind speed variations:

$$V_w = \begin{cases} 10 \text{ m/sec} & 0 < t < 1 \\ 14 \text{ m/sec} & 1 < t < 2 \\ 10 \text{ m/sec} & 2 < t < 3 \end{cases}$$

- SMC parameters: $\eta_1 = 0$, $K_{sw1} = 50$, $\varepsilon_1 = 0.01$
- NSMC parameters: $\lambda_1 = 219$, $\mu_1 = 1/3$, $\eta_1 = 0$, $K_{sw1} = 50$, $\varepsilon_1 = 0.01$
- FoNSMC parameters: $\alpha_1 = 0.3$, $\lambda_1 = 219$, $\mu_1 = 1/3$, $\eta_1 = 0$, $K_{sw1} = 50$, $\varepsilon_1 = 0.01$.

Some other common parameters among the three approaches are selected as:

$$\hat{a} = 7,\ \hat{b} = 10.5,\ \hat{c} = 0.05.$$

In addition, the PI controller parameters of the internal current-control-loops are considered as:

$$K_P = 1,\ K_I = 10.$$

Figure 4 WECS connected to the DC-grid, (a) generator mechanical speed (b)–(d) generator electrical torque (e)–(g) generator-side converter currents (h) THD of the generator-side converter current (see online version for colours)

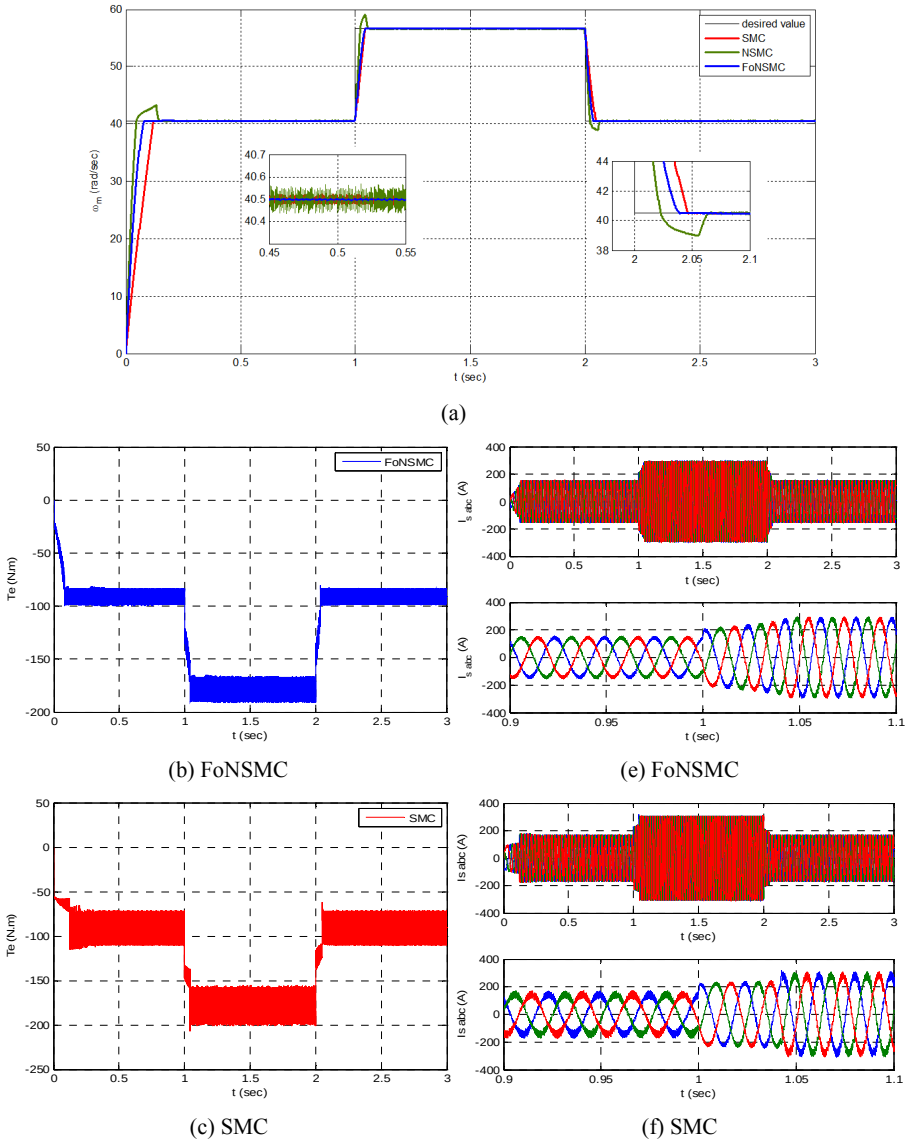

(a)

(b) FoNSMC

(e) FoNSMC

(c) SMC

(f) SMC

Figure 4 WECS connected to the DC-grid, (a) generator mechanical speed (b)–(d) generator electrical torque (e)–(g) generator-side converter currents (h) THD of the generator-side converter current (continued) (see online version for colours)

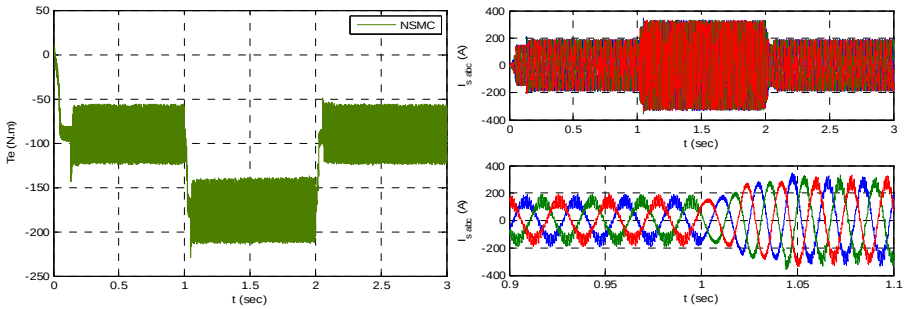

(d) NSMC (g) NSMC

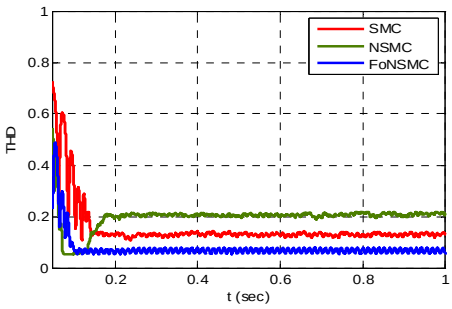

(h)

Generator mechanical speed, electrical torque, generator-side converter currents, and THD of the currents are presented in Figure 4. Figure 4(a) confirms that the mechanical speed tracks the optimal value for the three methods. But the SMC presents a slow response, and the NSMC shows large overshoot, while the FoNSMC has an enough fast response with small overshoot. In the other word, the FoNSMC is a balance between the SMC and the NSMC. In addition, the FoNSMC indicates small speed tracking error in comparison with the other methods. In Figures 4(b) to 4(g), the electrical torque and the generator currents are presented. From these figures, it is evident that the electrical torque and the generator currents have low chattering for the FoNSMC against the two other methods. Also based on Figure 4(h), the total harmonic distortion (THD) of the FoNSMC is lower than the SMC and the NSMC.

In the FoNSMC, the system convergence speed, overshoot and chattering are tunable by $0 < \alpha_1, \mu_1 < 1$ and λ_1 parameters. The mentioned parameters effects are discussed in below:

1 α_1: The system overshoot can be decreased by reducing the integral term $D^{-\alpha_1}$ of the sliding manifold (28) for small values of α_1. Also, small values of α_1 can increase the effect of the integral term $D^{-(1-\alpha_1)}$ in the control law (32), which is the main reason of decreasing the chattering. On the other hand, small values of α_1 can decrease convergence speed. As a result, determining a proper α_1 is a delicate matter and needs a trade-off.

2 μ_1: Small value of μ_1 improves the system convergence speed, while very small value ($\mu_1 \to 0$) can amplify the system chattering and it is not desirable.

3 λ_1: Effective value of λ_1 is achievable by simulation. But high values of λ_1 can magnify the PMSG current and electrical torque chattering.

5.2 WECS connected to the AC-grid

In this section, to examine the performance of the proposed FoNSMCs on both converters, the PMSG is connected to an AC-grid. Specifications of the proposed controllers are compared with the SMC and the results are presented in Figures 5 and 6.

Wind speed variations and the parameters of examined methods are selected as follows.

Wind speed variations:

$$V_w = \begin{cases} 10 \text{ m/sec} & 0.5 < t < 1 \\ 14 \text{ m/sec} & 1 < t < 1.5 \\ 12 \text{ m/sec} & 1.5 < t < 2 \end{cases}$$

- SMC parameters: $\eta_1 = 0$, $K_{sw1} = 50$, $\varepsilon_1 = 0.01$ and $\eta_2 = 100$, $K_{sw2} = 200$, $\varepsilon_2 = 0.01$
- FoNSMC parameters: $\alpha_1 = 0.3$, $\lambda_1 = 219$, $\mu_1 = 1/3$, $\eta_1 = 0$, $K_{sw1} = 50$, $\varepsilon_1 = 0.01$ and $\alpha_2 = 0.3$, $\lambda_2 = 200$, $\mu_2 = 1/3$, $\eta_2 = 100$, $K_{sw2} = 200$, $\varepsilon_2 = 0.01$.

The DC-link voltage, maximum captured power, mechanical speed, and THD of the grid-side currents are presented in Figure 5. Figure 5(a) demonstrates the DC-link voltage tracking. This figure confirms that the voltage tracking error of the FoNSMC is considerably lower than the SMC. In Figure 5(b), although the desired power is higher than the extracted power due to the turbine rotational and converters losses, but the maximum extracted power of the FoNSMC is higher than the SMC. For example at $t = 1.25$ sec., the maximum extracted power of the FoNSMC is 8000 W, while SMC's maximum power is 7600 W. As a result, the effectiveness of the FoNSMC is revealed by capturing 400 W extra power. From Figure 5(c), it is evident that the speed tracking error of the FoNSMC is small in comparison with the SMC. Figure 5(d) shows that the THD of the both methods is around 0.5% and is acceptable.

For more details, the active and reactive power, and the generator and grid-side converters currents of the SMC and the FoNSMC are presented in Figure 6. Finally, it is worthy to note that choosing the grid-side FoNSMC parameters is more delicate in comparison with the generator-side FoNSMC, and more attention is needed. For example, the grid-side controller is really sensitive to big sampling times and it can cause the reactive power oscillation.

Figure 5 WECS connected to the AC-grid, (a) DC-link voltage tracking ($V_{dc\text{-}ref}$ = 750 V) (b) active power delivered to the AC grid (c) generator mechanical speed (d) THD of the grid-side converter current (see online version for colours)

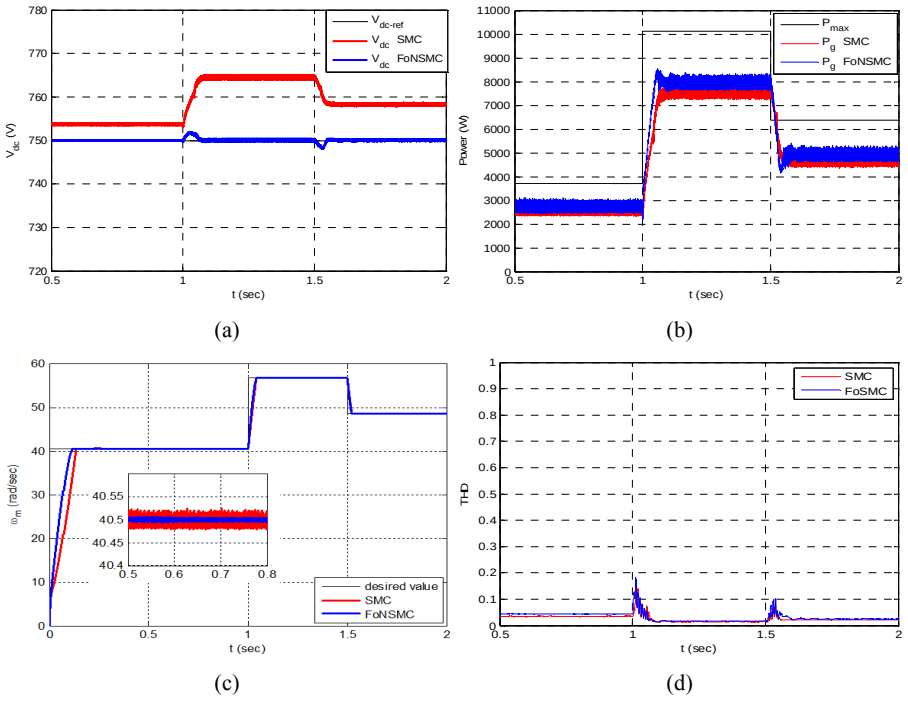

Figure 6 (a)–(b) Active and reactive power delivered to the AC-grid (c)–(d) Grid-side converter currents (see online version for colours)

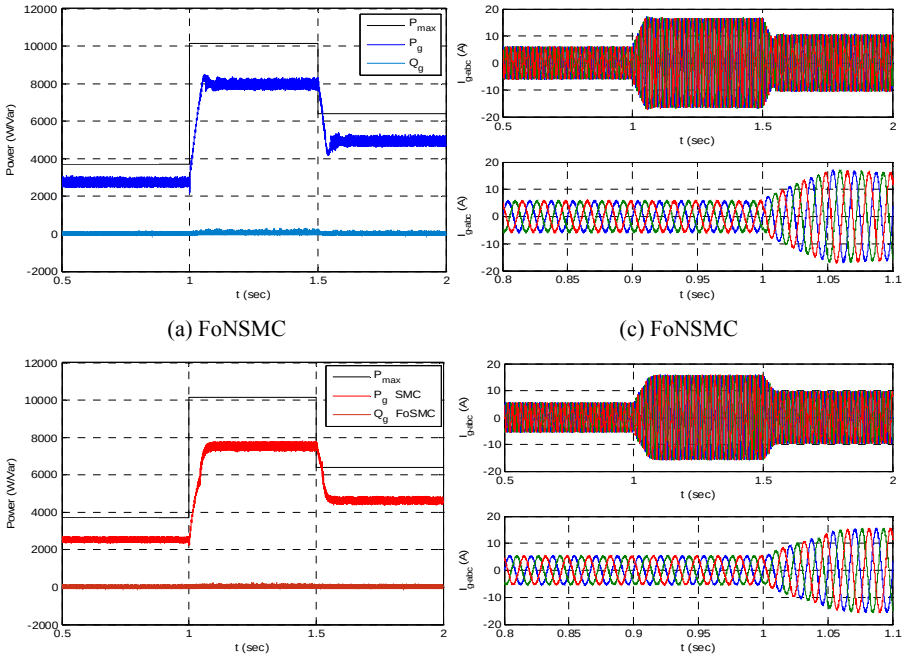

(a) FoNSMC (c) FoNSMC

(b) SMC (d) SMC

In addition, the internal current-control-loops parameters for the grid-side converter are considered as:

$$K_d = K_q = 400.$$

6 Conclusions

In this paper, two novel FoNSMC controllers have been developed for maximum power extraction of the PMSG-based WECS. The first controller sets the generator speed, and the second controller regulates the DC-link voltage. The proposed fractional controllers possess extra tuning parameters, which make them powerful to achieve fast and high precision responses. The controllers have been verified by fractional-order nonlinear stability theorems. The simulation results have shown the superiority of the proposed designs over the conventional SMC-based controllers.

References

Aghababa, M.P. (2013) 'A fractional-order controller for vibration suppression of uncertain structures', *ISA Trans.*, Vol. 52, No. 6, pp.881–887.

Aghababa, M.P. (2013) 'A switching fractional calculus-based controller for normal non-linear dynamical systems', *Nonlinear Dynam.*, Vol. 75, No. 3, pp.577–588.

Aissaoui, A.G., Tahour, A., Essounbouli, N., Nollet, F., Abid, M. and Chergui, M.I. (2013) 'A fuzzy-PI control to extract an optimal power from wind turbine', *Energy Convers. Manage*., Vol. 65, No. 1, pp.688–696.

Beltran, B., Ali, T.A. and El Hachemi Benbouzid, M. (2009) 'High-order sliding-mode control of variable-speed wind turbines', *IEEE Trans. Ind. Electron*., Vol. 56, No. 9, pp.3314–3321.

Benelghali, S., El Hachemi-Benbouzid, M., Charpentier, J.F., Ahmed-Ali, T. and Munteanu, I. (2011) 'Experimental validation of a marine current turbine simulator: application to a permanent magnet synchronous generator-based system second-order sliding mode control', *IEEE Trans. Ind. Electron*., Vol. 58, No. 1, pp.118–126.

Bianchi, F.D., De Battista, H.N. and Mantz, R.J. (2007) *Wind Turbine Control Systems: Principles, Modelling and Gain Scheduling Design*, Springer-Verlag, Berlin, Germany.

Cadenas, E. and Rivera, W. (2009) 'Short term wind speed forecasting in La Venta, Oaxaca, Mexico, using artificial neural networks', *Renew. Energy*, Vol. 34, No. 1, pp.274–278.

Cao, J., Ma, C., Jiang, Z. and Liu, S. (2011) 'Nonlinear dynamic analysis of fractional order | rub-impact rotor system', *Commun. Nonlinear Sci. Numer. Simulat*., Vol. 16, No. 3, pp.1443–1463.

Chang, Y.H., Wu, C., Chen, H.C., Chang, C.W. and Lin, H.W. (2011) 'Fractional-order integral sliding-mode flux observer for sensorless vector-controlled induction motors', *American Control Conference*, 29 June–1 July, San Francisco, USA, pp.190–195.

Chen, Y.Q. (2006) 'Ubiquitous fractional order controls', *Proceedings of the Second IFAC Workshop on Fractional Differentiation and its Applications*, Porto (ISEP), Portugal, pp.481–492.

Chinchilla, M., Arnaltes, S. and Burgos, J.C. (2006) 'Control of permanent-magnet generators applied to variable-speed wind-energy systems connected to the grid', *IEEE Trans. Energy Conver*., Vol. 21, No. 1, pp.130–135.

Corradini, M.L., Ippoliti, G. and Orlando, G. (2012) 'Fully sensorless robust control of variable-speed wind turbines for efficiency maximization', *Automatica*, Vol. 49, No. 10, pp.3023–3031.

Dadras, S. and Momeni, H.R. (2012) 'Fractional terminal sliding mode control design for a class of dynamical systems with uncertainty', *Commun. Nonlinear Sci. Numer. Simulat*., Vol. 17, No. 1, pp.367–377.

Efe, M.Ö. (2008) Fractional fuzzy adaptive sliding-mode control of a 2-DOF direct-drive robot arm', *IEEE Trans. Syst. Man. Cyb. B*, Vol. 38, No. 6, pp.1561–1570.

Eltamaly, A.M. and Farh, H.M. (2013) 'Maximum power extraction from wind energy system based on fuzzy logic control', *Electr. Pow. Syst. Res.,* Vol. 97, No. 1, pp.144–150.

Ezzat, M.A. (2011) 'Theory of fractional order in generalized thermoelectric MHD', *Appl. Math. Model*, Vol. 35, No. 10, pp.4965–4978.

Gafiychuk, V., Datsko, B. and Meleshko, V. (2008) 'Mathematical modeling of time fractional reaction-diffusion systems', *J. Comput. Appl. Math*., Vol. 220, Nos. 1–2, pp.215–225.

Hewitt, E. and Stromberg, K. (1965) *Real and Abstract Analysis,* Springer-Verlag, Berlin, Germany.

Kasem-Alaboudy, A.H., Daoud, A.A. Desouky, S.S. and Salem, A.A. (2012) 'Converter controls and flicker study of PMSG-based grid connected wind turbines', *Ain. Shams. Eng. J*., Vol. 4, No. 1, pp.75–91.

Laskin, N. (2000) 'Fractional market dynamics', *Physica A*, Vol. 287, Nos. 3–4, pp.482–492.

Li, C. and Deng, W. (2007) 'Remarks on fractional derivatives', *Appl. Math. Comput*., Vol. 187, No. 2, pp.777–784.

Li, S., Haskew, T.A., Swatloski, R.P. and Gathings, W. (2012) 'Optimal and direct-current vector control of direct-driven PMSG wind turbines', *IEEE Transactions on Power Electronics*, Vol. 27, No. 5, pp.2325–2337.

Li, Y., Chen, Y.Q. and Podlubny, I. (2010) 'Stability of fractional-order nonlinear dynamic systems: Lyapunov direct method and generalized Mittag-Leffler stability', *Comput. Math. Appl.*, Vol. 59, No. 5, pp.1810–1821.

Lin, W.M., Hong, C.M., Ou, T.C. and Chiu, T.M. (2011) 'Hybrid intelligent control of PMSG wind generation system using pitch angle control with RBFN', *Energy Convers. Manage*., Vol. 52, No. 2, pp.1244–1251.

Luo, Y., Chen, Y.Q. and Pi, Y. (2011) 'Experimental study of fractional order proportional derivative controller synthesis for fractional order systems', *Mechatronics*, Vol. 21, No. 1, pp.204–214.

Melicio, R., Mendes, V.M.F. and Catalao, J.P.S. (2010) 'Fractional-order control and simulation of wind energy systems with PMSG/full-power converter topology', *Energy Convers. Manage*., Vol. 51, No. 6, pp.1250–1258.

Morimoto, S., Nakamura, T. and Takeda, Y. (2005) 'Power maximization control of variable-speed wind generation system using permanent magnet synchronous generator', *Electr. Eng. Jpn.*, Vol. 150, No. 2, pp.11–19.

Petras, I. and Magin, R.L. (2011) 'Simulation of drug uptake in a two compartmental fractional model for a biological system', *Commun. Nonlinear Sci. Numer. Simulat*., Vol. 16, No. 12, pp.4588–4595.

Podlubny, I. (1999) *Fractional Differential Equations*, Academic Press, New York.

Qiao, W., Qu, L. and Harley, R.G. (2009) 'Control of IPM synchronous generator for maximum wind power generation considering magnetic saturation', *IEEE Trans. Ind. Appl.*, Vol. 45, No. 3, pp.1095–1105.

Qiao, W., Yang, X. and Gong, X. (2012) 'Wind speed and rotor position sensorless control for direct-drive PMG wind turbines', *IEEE Trans. Ind. Appl*., Vol. 48, No. 1, pp.3–11.

Shoja-Majidabad, S., Toosian-Shandiz, H. and Hajizadeh, A. (2014) 'Decentralized sliding mode control of fractional-order large-scale nonlinear systems', *Nonlinear Dynamics*, Vol. 77, Nos. 1–2, pp.119–134.

Tang, Y., Zhang, X., Zhang, D., Zhao, G. and Guan, X. (2012) 'Fractional-order sliding mode controller design for antilock braking systems', *Neurocomputing*, Vol. 111, No. 2, pp.122–130.

Thongam, J.S., Beguenane, R., Tarbouchi, M., Okou, A.F., Merabet, A., Fofana, I. and Bouchard, P. (2012) 'A rotor speed estimation algorithm in variable speed permanent magnet synchronous generator wind energy conversion system', *Int. J. Robust Nonlin.*, Vol. 23, No. 16, pp.1880–1890.

Uehara, A., Pratap, A., Goya, T., Senjyu, T., Yona, A., Urasaki, N. and Funabashi, T. (2011) 'A coordinated control method to smooth wind power fluctuations of a PMSG-based WECS', *IEEE Trans. Energy Conver*., Vol. 26, No. 2, pp.550–558.

Valenciaga, F. and Puleston, P.F. (2008) 'High-order sliding control for a wind energy conversion system based on a permanent magnet synchronous generator', *IEEE Trans. Energy Conver*., Vol. 23, No. 3, pp.860–867.

Yin, C., Stark, B., Chen, Y.Q. and Zhong, S.M. (2013) 'Adaptive minimum energy cognitive lighting control: integer order vs fractional order strategies in sliding mode based extremum seeking', *Mechatronics*, Vol. 23, No. 7, pp.863–872.

Zhang, B.T., Pi, Y.G. and Luo, Y. (2012) 'Fractional order sliding-mode control based on parameters auto-tuning for velocity control of permanent magnet synchronous motor', *ISA Trans.*, Vol. 51, No. 5, pp.649–656.

Appendix

Specifications of the wind turbine, DC-link and PMSG.

Table 1 Parameters of wind turbine

Parameter	*Value*
r (turbine blade length)	2 m
ρ (air density)	1.225 kg.m^3
λ_{opt} (optimal tip speed ratio)	8.1
$C_{\max}$ (maximum power coefficient)	0.48
β (pitch angle)	0 deg
V_W (wind speed cut-in and cut-off region)	[3 14] m/sec

Table 2 Parameters of PMSG, DC-link and grid filter

Parameter	*Value*
R_s (stator resistance)	0.00829 Ω
L_{sd} (stator direct inductance)	0.174 mH
L_{sd} (stator quadrature inductance)	0.174 mH
φ_f (permanent magnet flux)	0.071 Wb
p (number of pole pairs)	6
J (inertia)	0.089 kg.m^2
F (rotational damping term)	0.005 N.m.sec
C (DC-link capacitance)	6,000 μF
V_{dc} (DC-link voltage)	750 V
R_g (grid filter resistance)	0.02 Ω
L_g (grid filter inductance)	20 mH
$V_{g\ rms\ L\text{–}L}$ (grid voltage)	400 V
f_g (grid frequency)	60 Hz